Results in Chemistry 3 (2021) 100106

Contents lists available at ScienceDirect

Results in Chemistry

journal homepage: www.elsevier.com/locate/rechem

Photoactivatable 1,2-dioxetane chemiluminophores

Lucas S. Ryan [a], Andrew Nakatsuka [a], Alexander R. Lippert [a,b,c,*]

[a] Department of Chemistry, Southern Methodist University, Dallas, TX 75275-0314, USA
[b] Center for Drug Discovery, Design, and Delivery (CD4) Southern Methodist University, Dallas, TX 75275-0314, USA
[c] Center for Global Health Impact (CGHI), Southern Methodist University, Dallas, TX 75275-0314, USA

ARTICLE INFO

Keywords:
Chemiluminescence
Photoactivation
Spiropyran
1,2-dioxetanes
Photolabile protecting groups

ABSTRACT

Photochemical control of molecules has provided chemists with the ability to establish high spatiotemporal control of chemical configuration and activity. Herein, we report **UVC-454**, **UVA-454**, and **Spiro-CL** as photoactivatable chemiluminescence compounds. **UVC-454** and **UVA-454** are protected with *ortho*-nitrobenzyl protecting groups that provide irreversible photochemical uncaging of the chemiluminophore species through UV light irradiation. **UVC-454** and **UVA-454** can be selectively activated based on uncaging wavelength, and demonstrate ability to be photoactivated in water. **Spiro-CL** is a novel chemiluminescent spiropyran that can reversibly interconvert from its stable spiropyran form to a metastable merocyanine form through UV or visible light irradiation, respectively. Further, this compound exhibits chemiluminescence in its open form upon irradiation with UV light in DMSO.

Light and chemistry have a uniquely intertwined relationship, where light can be used to enact and enable control of chemical phenomena [1]. Photoswitches are one such class of molecules that can be precisely manipulated by light [2]. Light interacts with photoswitch structures by inducing reversible photochemical isomerization or bond formation/cleavage to metastable intermediates [3]. Rhodopsin is one such naturally occurring photoswitch that enables vision in animals [4] and photosynthesis for some archaea [5]. Furthermore, synthetically devised photoswitches such as azobenzenes and stilbenes have been implemented for controlling both structure and expression of biomacromolecules [6–8]. Spiropyrans are another type of photoswitch that has unique properties as compared to others in its class [9]. The spiropyran converts from a relatively non-polar, non-fluorescent spiropyran (SP) form to an open merocyanine (MC) chromophore, coinciding with a large shift in the molecule's polarity in zwitterionic form. While the MC chromophore shows higher absorbance than the closed SP form, it exhibits moderate fluorescence in polar solvents and is virtually non-fluorescent in water. However, encapsulation [10] or incorporation into polymers [11–13], nanodots [14], and thin films [15] has granted major improvements in fluorescence efficiency. Spiropyrans have been largely implemented for dynamic fluorescence due to increased fluorescence quantum yield that arises from conformational restraint and minimization of solvent-based quenching, as well as innate thermochromic [16], acidochromic [17], solvatochromic [18], electrochromic, [19] and mechanochromic [12,20,21] properties.

Light can also initiate irreversible photochemical processes. Photolabile protecting groups (PPGs) are an established method to cage compound activity through covalent attachment of a photolabile group, allowing for buildup of the substrate in regions of interest and high spatiotemporal control for the release of a substrate through photochemical bond cleavage. Development of photoremovable groups has been of particular interest over the last half century, and its study has garnered a diverse array of new PPGs exhibiting a wide range of uncaging mechanisms, uncaging wavelengths, and functional group compatibility. Some PPGs include phenacyl [22–24], nitroaryl [25–29], coumarinyl [30,31], BODIPY [32–37], and cyanine [38] derivatives. Of this class, ortho-nitrobenzyl protecting groups exhibit uncaging capability in both the UV and NIR regions through single and two photon [28,29] mechanisms, respectively, and have been implemented in a wide range of applications, including natural product synthesis [39,40], caged ATP [41], RNA [42], DNA [42], and peptide [43] synthesis, prodrug release [44–46], and others.

Activity-based sensing (ABS) relies on the use of caged luminophores that are uncaged based on selective cleavage of protecting groups to obtain a readout [47]. Common ABS detection techniques use optical readouts including absorption, NMR, optoacoustic [48–50], fluorescence [51–53], and chemiluminescence-based agents

* Corresponding author at: Department of Chemistry, Southern Methodist University, Dallas, TX 75275-0314, USA.
E-mail address: alippert@smu.edu (A.R. Lippert).

https://doi.org/10.1016/j.rechem.2021.100106
Received 14 November 2020; Accepted 27 January 2021

[54]. Chemiluminescence provides many advantages over other optical reporters, including high turn-on and increased depth penetration, while obviating the need for external excitation [55]. Specifically, 1,2-dioxetanes have been established as critical chemiluminescence-based ABS reporter substrates, as they provide a facile and functional means of caging luminescent emission through protection of the dioxetane phenol with a reactive handle. Subsequent interaction with the analyte of interest will uncage the dioxetane phenol, initiating an electron exchange luminescence (CIEEL) process to generate photonic emission [56–60]. This strategy has been used for activity-based detection and quantification of various substrates [61–71].

A key challenge for *in vivo* chemiluminescence imaging is attaining good spatiotemporal control of the luminescent signal for localization and maximizing total luminescent output. Utilization of photocaged chemiluminescent compounds can ultimately circumvent this issue by localizing chemiluminescence signal to the point of illumination. Herein, we report the use of both irreversible and reversible photoinitiated uncaging of 1,2-dioxetane chemiluminophores as a fundamental step towards this goal. We synthesized *ortho*-nitrobenzyl protected dioxetanes **UVC-454** and **UVA-454** that can be irradiated by UVC (254 nm) and UVA (365 nm) light, respectively to emit luminescence at 454 nm. We also report the first chemiluminescent spiropyran compound **Spiro-CL** that undergoes reversible opening to its MC form under UV light, and exhibits chemiluminescence in DMSO (Scheme 1).

1. Material and methods

1.1. Synthetic procedures

General synthetic materials and methods. All reactions were performed in dried glassware under an atmosphere of dry N_2. Silica gel P60 (SiliCycle) was used for column chromatography and SiliCycle 60 F254 silica gel (precoated sheets, 0.25 mm thick) was used for analytical thin layer chromatography. Plates were visualized by fluorescence quenching under UV light. Other reagents were purchased from Sigma-Aldrich (St. Louis, MO), Alfa Aesar (Ward Hill, MA), EMD Millipore (Billerica, MA), Oakwood Chemical (West Columbia, SC), Beantown Chemical (Hudson, NH), and Cayman Chemical (Ann Arbor, MI) and used without further purification. ^{1}H NMR for compounds and ^{13}C NMR for compounds were collected on a Bruker 400 MHz or a JEOL 500 MHz spectrometer in the Department of Chemistry at Southern Methodist University. ^{1}H and ^{13}C NMR spectra for characterization of new compounds and monitoring reactions were collected in $CDCl_3$ (Cambridge Isotope Laboratories, Cambridge, MA). All chemical shifts are reported in the standard notation of parts per million using the peak of residual proton signals of the deuterated solvent as an internal reference. Coupling constant units are in Hertz (Hz). Splitting patterns are indicated as follows: br, broad; s, singlet; d, doublet; t, triplet; q, quartet; m, multiplet; dd, doublet of doublets; dt, doublet of triplets. Low resolution mass spectrometry was performed on an Advion Expression^L CMS (ESI source) at Southern Methodist University. High resolution mass spectroscopy was performed on a Shimadzu IT-TOF (ESI source) at the Shimadzu Center for Advanced Analytical Chemistry at the University of Texas, Arlington.

(1*r*,3*r*,5*R*,7*S*)-2-((4-chloro-3-((2-nitrobenzyl)oxy)phenyl)(methoxy)methylene)adamantane (2). To an oven-dried 50 mL roundbottom flask, 5-(((1r, 3r, 5R, 7S)-adamantan-2-ylidene) (methoxy) methyl)-2-chlorophenol [72] (441 mg, 1.45 mmol, 1.0 equiv) and 24 mL anhydrous THF were added and cooled to 0 °C. Diethylazodicarboxylate (0.54 mL, 3.48 mmol, 2.4 equiv) was added. Triphenyl phosphine (663 mg, 1.74 mmol, 1.2 equiv) was dissolved in 3 mL anhydrous THF was added dropwise over 5 min. The reaction was stirred for 2 hr until completion as determined by TLC. The crude contents were washed with saturated NH_4Cl, extracted with 3 × 25 mL EtOAc, dried with Na_2SO_4, filtered, and concentrated under vacuum. Column chromatography (1% EtOAc/Hexanes) yielded **2** (307 mg, 0.70 mmol, 48%). ^{1}H NMR δ 8.23 (d, 1H, J = 7.6 Hz), 8.09 (d, 1H, J = 7.6 Hz) 7.74 (t, 1H, J = 7.6 Hz), 7.52 (t, 1H, J = 7.6 Hz), 7.39 (d, 1H, J = 8.0 Hz), 6.98 (s, 1H), 6.93 (m, 1H), 5.59 (s, 2H), 3.30 (s, 3H), 2.25 (s, 1H), 1.76–1.99 (m, 11*H*). ^{13}C NMR (100 MHz, $CDCl_3$) δ 153.2, 142.4, 135.5, 134.3, 133.6, 132.9, 130.0, 128.4, 128.4, 125.1, 123.1, 121.9, 114.5, 67.5, 39.1, 39.0, 37.1, 32.4, 30.3, 28.2. LRMS for $C_{25}H_{26}ClNO_4$ $[M + H]^+$ found 440.2.

(1r,3r,5R,7S)-2-((4-chloro-3-((4,5-dimethoxy-2-nitrobenzyl)oxy)phenyl)(methoxy)methylene)adamantane (3). To an oven-dried 50 mL roundbottom flask, 5-(((1r, 3r, 5R, 7S)-adamantan-2-ylidene) (methoxy) methyl)-2-chlorophenol [72] (158 mg, 0.52 mmol, 1.0 equiv) and 5 mL anhydrous THF were added and cooled to 0 °C. Diethylazodicarboxylate (0.09 mL, 0.62 mmol, 1.2 equiv) was added. Triphenyl phosphine (164 mg, 0.624 mmol, 1.2 equiv) dissolved in 1 mL anhydrous THF was added dropwise over 5 min. The reaction was stirred for 2 hr until completion as determined by TLC. The crude contents were washed with saturated NH_4Cl, extracted with 3 × 25 mL EtOAc, dried with Na_2SO_4, filtered, and concentrated under vacuum. Column chromatography (1–5% EtOAc/Hexanes) yielded **3** (166 mg, 0.33 mmol, 64%). ^{1}H NMR (400 MHz, $CDCl_3$) δ 7.82 (s, 1H), 7.71 (s, 1H), 7.40 (d, 1H, J = 8.0 Hz), 7.06 (d, 1H, J = 1.2 Hz), 6.93 (dd, 1H, J_1 = 8.0 Hz, J_2 = 1.2 Hz), 5.57 (s, 2H), 4.04 (s, 3H), 4.00 (s, 3H), 3.32 (s, 3H), 3.26 (s, 1H), 2.62 (s, 1H)

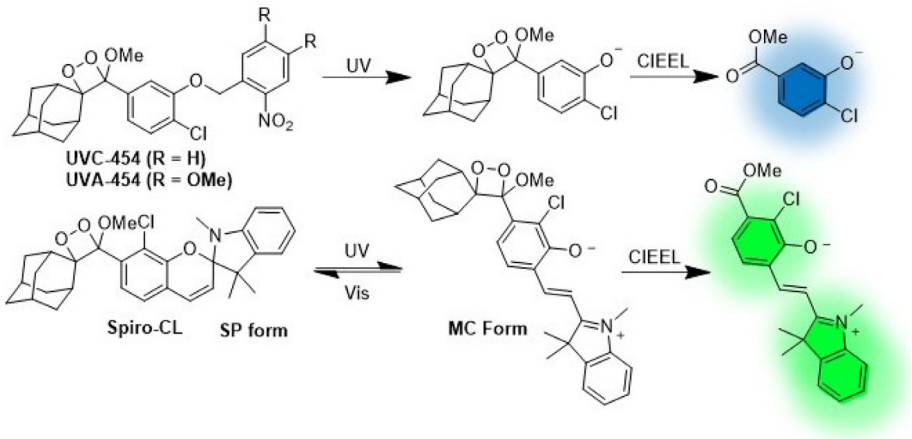

Scheme 1. Design of photoactivatable chemiluminescence compounds.

1.79–2.00 (m, 11*H*). ^{13}C NMR (100 MHz, $CDCl_3$) δ 154.1, 153.2, 147.8, 142.4, 138.7, 135.7, 133.0, 129.8, 129.2, 123.1, 121.7, 114.6, 109.5, 107.9, 67.6, 56.5, 56.4, 39.1, 39.0, 37.1, 32.4, 30.3, 28.2. LRMS for $C_{27}H_{23}ClNO_6$ $[M + H]^+$ found 500.2.

(1*r*,3*r*,5*r*,7*r*)-4′-(4-chloro-3-((2-nitrobenzyl)oxy)phenyl)-4′-methoxyspiro[adamantane-2,3′-[1,2]dioxetane] (UVC-454). In a 2-neck roundbottom flask, Compound **2** (50 mg, 0.12 mmol) was dissolved in 3 mL THF. Rose bengal (8 mg, 0.0082 mmol) was added. Upon cooling to 0 °C, O_2 was bubbled into the solution the solution and the flask was irradiated under white light for 1 hr. Upon completion as determined by TLC, the crude was evaporated onto silica and loaded for column chromatography in 5% EtOAc/Hexanes, yielding **UVC-454** (4.4 mg, 0.008 mmol, 35%) as a mixture of diastereomers ^{1}H NMR (500 MHz, $CDCl_3$) δ 8.12 (d, 1H, J = 1.1 Hz), 7.92 (d, 1H, J = 1.1 Hz), 7.63 (m, 2H) 7.40–7.45 (m, 4H), 5.54 (s, 2H), 3.12 (s, 3H), 2.93 (s, 1H), 1.71–1.91 (m, 12H). ^{13}C NMR (125 MHz, $CDCl_3$) δ 146.8, 135.0, 134.1, 133.0, 130.3, 128.6, 125.1, 111.4, 95.4, 67.6, 49.9, 36.3, 34.7, 33.1, 31.6, 25.9, 25.8, 14.2. HRMS calcd for $C_{25}H_{26}ClNO_6$ $[M + Na]^+$ 494.1341, found 494.1854.

(1*r*,3*r*,5*r*,7*r*)-4′-(4-chloro-3-((4,5-dimethoxy-2-nitrobenzyl)oxy)phenyl)-4′-methoxyspiro[adamantane-2,3′-[1,2]dioxetane] (UVA-454). In a 2-neck roundbottom flask, Compound **3** (45 mg, 0.09 mmol) was dissolved in 3 mL THF. Rose bengal (12 mg, 0.012 mmol) was added. Upon cooling to 0 °C, O_2 was bubbled into the solution the solution and the flask was irradiated under white light for 3 hr. Upon completion as determined by TLC, the crude was evaporated onto silica and loaded for column chromatography in 5% EtOAc/Hexanes, yielding **UVA-454** (30 mg, 0.056 mmol, 63%). ^{1}H NMR (500 MHz, $CDCl_3$) δ 7.73 (s, 1H), 7.52 (s, 1H), 7.40 (s, 1H), 7.19 (m, 2H), 3.93 (s, 3H), 3.91 (s, 3H), 3.15 (s, 3H), 2.93 (s, 1H), 1.61–1.93 (m, 12H). ^{13}C NMR (125 MHz, $CDCl_3$) δ 154.1, 147.9, 138.9, 135.3, 130.2, 128.5, 111.5, 109.5, 107.9, 95.4, 67.7, 56.5, 56.4, 53.5, 50.0, 36.3, 34.8, 33.2, 33.1, 32.3, 31.6, 31.5, 29.7, 26.0, 25.9. HRMS calcd for $C_{27}H_{30}ClNO_8$ $[M + Na]^+$ 554.1552, found 554.2159.

4-(((1*r*,3*r*,5*R*,7*S*)-adamantan-2-ylidene)(methoxy)methyl)-3-chloro-2-hydroxybenzaldehyde (4). [65] In an oven-dried 3 mL pressure flask, 3-(((1*r*,3*r*,5*R*,7*S*)-adamantan-2-ylidene)(methoxy)methyl)-2-chloro-6-iodophenol [64] (600 mg, 1.39 mmol, 1 equiv), *N*-formylsaccharine (441 mg, 2.09 mmol, 1.5 equiv), Na_2CO_3 (221 mg, 2.09 mmol, 1.5 equiv), $Pd(OAc)_2$ (9.4 mg, 0.042 mmol, 0.03 equiv), and 1,4-bis(diphenylphosphino)butane (26 mg, 0.062 mmol, 0.045 equiv) were added, and purged 3x with N_2. 4 mL of anhydrous DMF was added, followed by anhydrous triethylsilane (0.29 mL, 1.81 mmol, 1.3 equiv). The reaction was capped and pre-stirred for 10 min, then brought up to 80 °C and stirred for 16 hr. The reaction was taken off heat and allowed to cool to RT, washed with saturated NH_4Cl, extracted with 3 × 25 mL EtOAc, dried with Na_2SO_4, filtered, and concentrated under vacuum. Column chromatography (10% EtOAc/Hexanes) yielded **4** (253 mg, 0.76 mmol, 76%) as a yellow solid. ^{1}H NMR (500 MHz, $CDCl_3$) δ 11.63 (s, 1H), 9.90 (s, 1H), 7.48 (d, 1H, J = 7.4 Hz), 6.97 (d, 1H, J = 7.4 Hz), 3.33 (s, 3H), 3.30 (s, 1H), 1.6–2.12 (m, 12H).

7-(((1*r*,3*r*,5*R*,7*S*)-adamantan-2-ylidene)(methoxy)methyl)-8-chloro-1′,3′,3′-trimethylspiro[chromene-2,2′-indoline] (5). In a 2-neck roundbottom flask, Compound **4** (32 mg, 0.097 mmol, 1.0 equiv) and 1,3,3-trimethyl-2-methyleneindoline (0.02 mL, 0.097 mmol, 1.0 equiv) were dissolved in 4 mL pure EtOH under nitrogen atmosphere. The reaction was heated to 90 °C and refluxed for 5 hr. Upon completion as determined by TLC and ESI-MS, the reaction was washed in brine, extracted with 3 × 10 mL EtOAc, and concentrated under vacuum. Column chromatography (2% EtOAc/hexanes) yielded **5** (14 mg, 0.029 mmol, 30%). ^{1}H NMR (400 MHz, $CDCl_3$) δ 7.17 (t, 1H, J = 7.2 Hz), 7.08 (d, 1H, J = 7.2 Hz), 6.95 (d, 1H, J = 7.6 Hz), 6.85 (m, 2H), 6.75 (d, 1H, J = 8.0 Hz), 6.55 (d, 1H, J = 7.6 Hz), 5.76 (d, 1H, J = 10.0 Hz), 3.15–3.32 (m, 6H), 2.77 (d, 3H, J = 7.2 Hz), 2.20 (s, 6H), 1.21–1.89 (m, 12H). ^{13}C NMR (100 MHz, $CDCl_3$) δ 136.6, 135.8, 131.1, 128.7, 127.5, 123.9, 122.9, 121.4, 121.1, 120.7, 119.6, 119.2, 106.8, 56.9, 52.0, 51.8, 39.2, 39.1, 38.6, 37.2, 34.7, 32.9, 30.9, 29.7, 29.6, 29.0, 28.5, 28.3, 26.9, 25.7, 25.3, 22.7, 20.3, 14.4. LRMS for $C_{31}H_{34}ClNO_2$ $[M + H]^+$ found 488.3.

8-chloro-7-((1*r*,3*r*,5*r*,7*r*)-4′-methoxyspiro[adamantane-2,3′-[1,2]dioxetan]-4′-yl)-1′,3′,3′-trimethylspiro[chromene-2,2′-indoline] (Spiro-CL). In a 2-neck roundbottom flask, Compound **5** (12.1 mg, 0.024 mmol) was dissolved in DCM. Methylene blue (3.5 mg, 0.011 mmol) was added. Upon cooling to 0 °C, O_2 was bubbled into the solution the solution and the flask was irradiated under yellow light for 1 hr. Upon completion as determined by ESI-MS, the crude was evaporated onto silica and loaded for column chromatography in 2% EtOAc/Hexanes, yielding **Spiro-CL** (4.4 mg, 0.008 mmol, 35%) as a mixture of diastereomers ^{1}H NMR (400 MHz, $CDCl_3$) δ 7.58 (d, 1H, J = 7.6 Hz), 7.18 (t, 1H, J = 7.6 Hz), 7.07 (m, 2H), 6.87 (m, 2H), 6.56 (dd, 1 Hz, J_1 = 7.6 Hz, J_2 = 5.2 Hz), 5.82 (t, 1H, J = 11.8 Hz), 3.22 (d, 3H, J = 12.4 Hz), 2.98 (s, 1H), 2.69–2.81 (d, 3H), 2.28 (d, 1H), 2.03 (d, 1H), 1.84 (m, 2H), 1.71 (m, 2H), 1.63 (s, 6H) 1.3–1.8 (m, 4H). ^{13}C NMR (100 MHz, $CDCl_3$) δ 150.7, 150.5, 148.1, 147.7, 136.5, 136.3, 132.7, 128.5, 127.6, 124.1, 122.7, 121.7, 121.4, 121.4, 121.2, 119.4, 119.3, 118.9, 122.1, 106.9, 106.8, 106.1, 105.4, 96.3, 42.4, 51.8, 49.7, 49.6, 36.7, 33.7, 33.5, 32.3, 32.2, 31.6, 31.4, 29.7, 29.1, 28.7, 26.2, 25.9, 25.8, 25.5, 20.2, 20.0, 14.1. HRMS calcd for $C_{31}H_{34}ClNO_4$ $[M + H]^+$ 520.2249, found 520.2796.

UVC-454 and UVA-454 irradiation in DMSO. Samples of **UVC-454** and **UVA-454** were dissolved to a concentration of 10 mM in DMSO in a 20-dram vial. The vial contents were irradiated by placing the vial directly in front of a Hitachi F-7000 fluorescence spectrophotometer Xe lamp source with 20 nm slit widths, and irradiated with 254, 365, and 488 nm light. A portion of the irradiated sample was then transferred into a cuvette containing 20 mM PBS pH 7.4 buffer with 10% Emerald II® to make a final concentration of 50 μM **UVC-454** or **UVA-454**. Luminescence was measured using a Hitachi F-7000 fluorescence spectrophotometer from 0 to 180 min, and readings were taken every 20 min. For luminescence kinetics experiments, samples of 1 mM **UVC-454** or **UVA-454** dissolved in DMSO were placed atop a Spectroline® ENF-240C UV lamp and irradiated with 254 nm or 365 nm for 30 min. 50 μL of the irradiated sample were immediately transferred 20 mM PBS pH 7.4 buffer with 10% Emerald II® to make a final concentration of 50 μM **UVC-454** or **UVA-454**. Luminescence was measured using a Hitachi F-7000 fluorescence spectrophotometer for 5 hr.

***In vitro* chemiluminescence response of UVC-454 to irradiation in aqueous media.** Samples of **UVC-454** and **UVA-454** were dissolved to give 100 mM solutions in DMSO. Aliquots of **UVC-454** and **UVA-454** were then transferred into a cuvette containing 20 mM PBS pH 7.4 buffer containing 10% Emerald II® solution to give a final concentration of 100–1000 μM **UVC-454** and 5% DMSO. The solution was irradiated by placing the cuvette in the cuvette holder of a Hitachi F-7000 fluorescence spectrophotometer Xe lamp source with 20 nm slit widths, and irradiated for 180 min. Chemiluminescence readings were taken every 20 min.

Monitoring Spiro-CL photoswitching using absorption spectroscopy. Absorbance spectra of **Spiro-CL** were collected using a Beckman Colter DU 800 spectrophotometer scanning from 200 to 800 nm, wavelength interval of 1.0 nm, and scan speed of 1200 nm/min. For solutions in EtOH, 100 μM **Spiro-CL** were dissolved in 200 proof EtOH and added to a cuvette. An initial absorbance read at t = 0 was taken, then the cuvette was taken out of the spectrophotometer and irradiated with 254 nm light from a Spectroline® ENF-240C UV lamp for 2 min. This process was repeated until t = 20 min. Then, the solution was irradiated with white light using a 120 W lamp (Home Depot, Dallas, TX) for 2 min, and an absorbance read was taken, and this process was repeated until t = 30 min. For

solutions in DMSO, 10 μM **Spiro-CL** was dissolved in DMSO and added to a cuvette. The cuvette was then irradiated with 254 nm light from a Spectroline® ENF-240C UV lamp for 2 min, and repeated for 20 min.

Monitoring fluorescence of Spiro-CL before and after irradiation. Fluorescence measurements were taken using a Hitachi F-7000 fluorescence spectrophotometer via the fluorescence detection mode. Fluorescence excitation and emission spectra were acquired with a slit widths of 5.0 nm. 10 μM **Spiro-CL** was dissolved in 200 proof EtOH, and fluorescence excitation and emission spectra were taken before irradiation of the sample with UV light. For the t = 0 fluorescence excitation read, the emission wavelength was set to 330 nm, and the excitation range was scanned from 200 to 320 nm. For the t = 0 fluorescence emission read, the excitation wavelength was set to 269 nm, and emission range was set from 279 to 600 nm. Then, the sample was taken out of the fluorometer and irradiated with 254 nm light from a Spectroline® ENF-240C UV lamp for 20 min. After irradiation, fluorescence excitation and emission reads were retaken. For the t = 20 min fluorescence excitation read, the emission wavelength was set to 525 nm, and the excitation range was scanned from 200 to 515 nm. For the t = 20 min fluorescence emission read, the excitation wavelength was set to 410 nm, and emission range was set from 420 to 600 nm.

Chemiluminescence of Spiro-CL. Chemiluminescence measurements were taken using a Hitachi F-7000 fluorescence spectrophotometer via the fluorescence detection mode. Fluorescence excitation and emission spectra were conducted with slit widths of 20 nm. solutions of 10 μM **Spiro-CL** were dissolved in 200 proof EtOH or pure DMSO and transferred into a cuvette. Then, the solutions were irradiated for t = 16 min using the 254 nm light source from a Spectroline® ENF-240C UV lamp. chemiluminescence measurements were taken at t = 0 and 16 min.

2. Results

2.1. Synthesis and in vitro response of UVC-454 and UVA-454

Both **UVC-454** and **UVA-454** were synthesized from literature reported precursor **1** [71,73] through Mitsunobu couplings with 2-nitrobenzyl alcohol (**UVC-454**) and 4,5-dimethoxy-2-nitrobenzyl alcohol (**UVA-454**) to make ethers **2** and **3**, followed by a [2 + 2] cycloaddition with $^1O_2$ via sensitization with Rose bengal to make the final photocaged dioxetane compounds (Scheme 2). Upon synthesis of the photocaged compounds, we proceeded to test their photoactivation capabilities (Fig. 1). Solutions of 10 mM concentrations of **UVC-454** or **UVA-454** in DMSO were irradiated with 254, 365, and 488 nm light for 180 min, and aliquots were transferred into 20 mM PBS pH 7.4 buffer containing 10% Emerald II® enhancer solution to give a final concentration of 50 μM. Fig. 1A and 1C show the luminescence emission response of **UVC-454** and **UVA-454** to uncaging with UVC and UVA light, respectively. Both give off bright luminescence, with emission peaks centered at 454 nm from the chemiluminescent scaffold, and 540 nm through energy transfer to Emerald II®. **UVC-454** gives an overall brighter response than **UVA-454** at 254 nm and 365 nm uncaging wavelengths, however, **UVA-454** showed a statistically significant difference in the uncaging response at its respective uncaging wavelength of 365 nm over 180 min as compared to 254 nm and 488 nm (Fig. 1D). Utilizing 254 nm light versus 365 nm light with **UVC-454** did not show a statistically significant response, however the uncaging response was statistically significant as compared photoinitiated cleavage using 488 nm light (Fig. 1B). The kinetics of luminescence emission of 50 μM **UVC-454** and **UVA-454** were taken after 30 min of 254 or 365 nm irradiation, respectively (Fig. 1E, 1F). Both probes show luminescence maxima at t = 0 with exponential luminescence decay baseline over 5 hr. We also controlled for uncaging due to thermolysis with **UVC-454** (Figure S1). The agent showed a small but steady luminescence output due to heating of the sample. We also tested the uncaging response **UVC-454** directly in aqueous media (Fig. 2), where 100 μM to 1 mM solutions of **UVC-454** in 20 mM PBS pH 7.4 buffer containing 10% Emerald II® solution were prepared and irradiated with 254 nm light for 180 min. Relatively low luminescence output was seen from both the 100 μM and 500 μM concentrations over the 180 min time period, but could be readily seen at the 750 μM and 1 mM concentrations.

2.2. Synthesis and in vitro response of Spiro-CL

Spiropyrans are synthesized through condensation of indoline compounds to salicylaldehydes. Due to the structural similarities between the spiropyrans and reported chemiluminescent salicylaldehyde precursor, [65] we decided to explore the possibility of developing a chemiluminescence photoswitch, where we utilize the CL scaffold as the chromene portion of the spiropyran. We first synthesized aldehyde **4** via a palladium catalyzed formylation method [74] in 85% yield (Scheme 3). We then appended 1,3,3-trimethyl-2-methyleneindoline to this structure through condensation to form the spiropyran precursor **5** in 30% yield. Finally, the enol ether underwent a [2 + 2] cycloaddition with $^1O_2$ generated by photosensitizer methylene blue under white light to generate **Spiro-CL** in 35% yield.

Upon synthesis of **Spiro-CL**, we began to examine its photoswitching capabilities. We first monitored changes in its absorbance to examine the effect of UV light irradiation on the sample. A 100 μM sample of **Spiro-CL** was irradiated for 20 min with a 254 nm light source and absorbance was measured every two minutes during that time period (Fig. 3). The absorbance spectra show clear increases in absorbance with the growth of a peak from 0 min to 20 min centered at 418 nm, indicating changes in the absorbance profile of the compound upon UV radiation. After the 20-minute UV irradiation period, the solution was irradiated for 10 min with a white light source and absorbance was monitored every two minutes. Absorbance at 418 nm decreased down to a steady state of around 0.06 absorbance units for the sample.

We then monitored changes in the fluorescence and chemiluminescence profiles of **Spiro-CL** due to UV light exposure (Fig. 4). A 10 μM solution of **Spiro-CL** in EtOH was subjected to fluorescence excitation and emission measurements before and after irradiation with UV light (Fig. 4A). Before irradiation, **Spiro-CL** exhibits fluorescence excitation and emission peaks centered at 290 nm and 350 nm, respectively. After 20 min of irradiation with the UV source, the excitation profile of the spiropyran broadens, with excitation maxima located at 260,

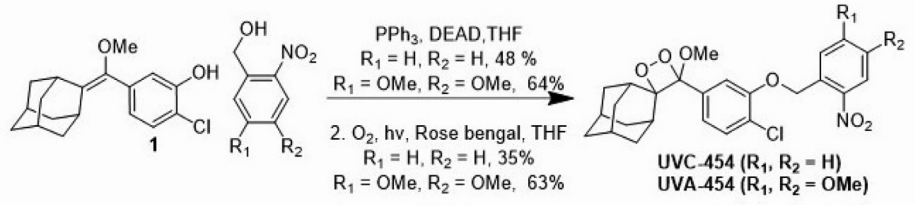

Scheme 2. Synthesis of UVC-454 and UVA-454.

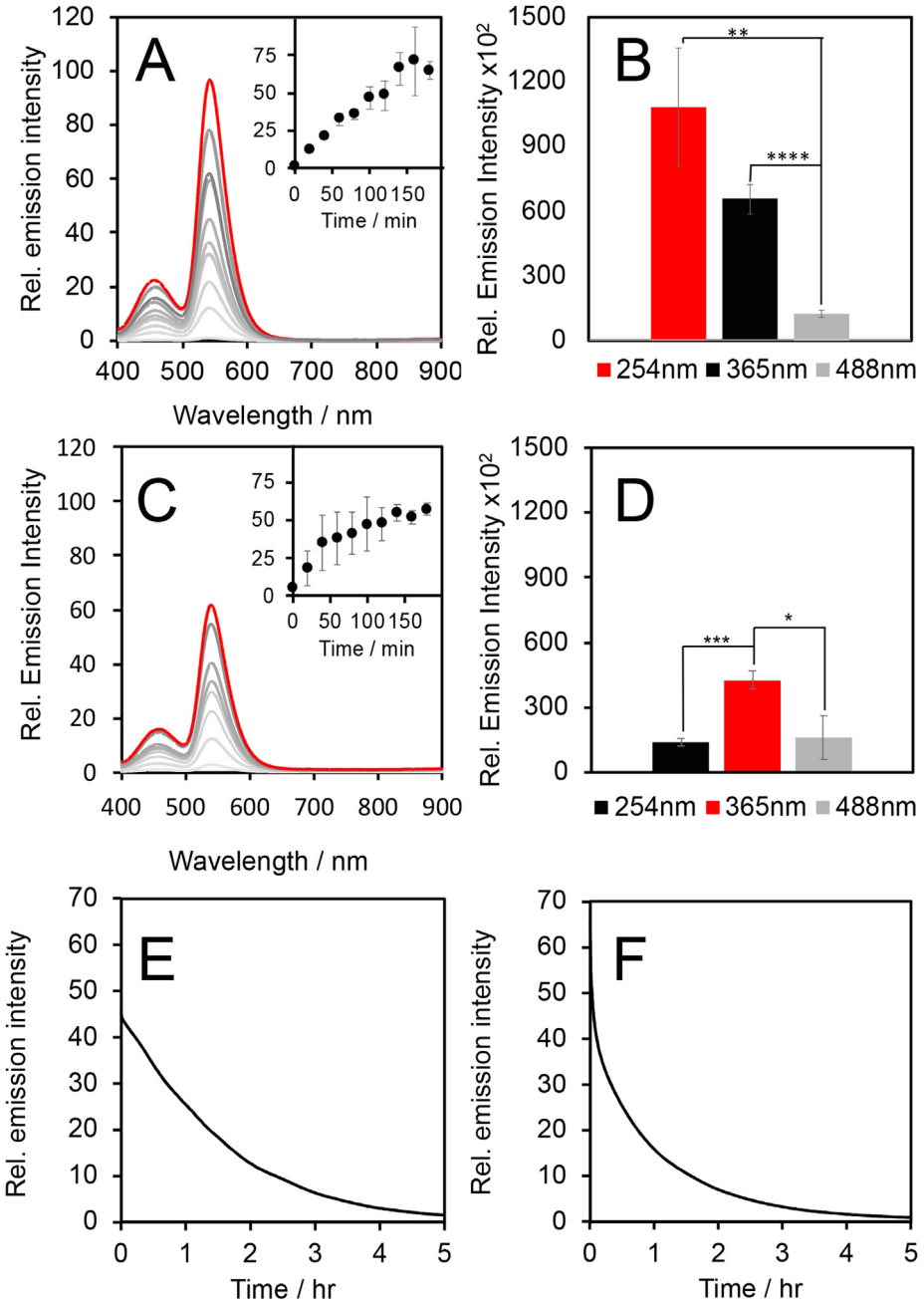

Fig. 1. Photoactivation of UVC-454 and UVA-454 in DMSO with 254 nm, 365 nm, and 488 nm irradiation (A) Plot of relative emission intensities of 50 μM **UVC-454** in PBS 7.4 buffer and 10% Emerald II® irradiated with 254 nm for 0–180 min. Inlay denotes emission intensity at 545 nm over 180 min. (B) Integrated emission intensities at 545 nm of 50 μM **UVC-454** in PBS 7.4 buffer and 10% Emerald II irradiated with 254 nm (red), 365 nm (black), and 488 nm (gray) light over 180 min. (C) Plot of relative emission intensities of 50 μM **UVA-454** in PBS 7.4 buffer and 10% Emerald II® irradiated with 365 nm for 0–180 min. Inlay denotes emission intensity at 545 nm over 180 min. (D) Integrated emission intensities at 545 nm of 50 μM **UVA-454** in PBS 7.4 buffer and 10% Emerald II irradiated with 254 nm (red), 365 nm (black), and 488 nm (gray) light over 180 min. Error bars are ± SD. Statistical significance was assessed using a two-tailed Student's *t* test. *$p < 0.05$ (n = 3 technical replicates), **$p < 0.005$ (n = 3 technical replicates), ***$p < 0.0005$ (n = 3 technical replicates), ****$p < 0.00005$ (n = 3 technical replicates). (E) Time course of chemiluminescence emission of 50 μM **UVC-454** at 545 nm irradiated with 254 nm light for 30 min. (F) Time course of chemiluminescence emission of 50 μM **UVA-454** at 545 nm irradiated with 365 nm light for 30 min. (For interpretation of the references to colour in this figure legend, the reader is referred to the web version of this article.)

350, and 450 nm. Fluorescence emission spectra after irradiation red-shifted to a peak centered around 540 nm. Finally, we tested the ability of the compound to exhibit chemiluminescence due to UV light-mediated opening of the luminophore (Fig. 4B). We subjected 10 μM **Spiro-CL** in DMSO to irradiation with a 254 nm light source and monitored chemiluminescence emission from the sample for 16 min. After 16 min, a small peak centered at 510 nm arose, indicating that the ring opening process mediated by UV irradiation enabled luminescence emission from the open MC form.

3. Discussion and conclusion

In conclusion, we synthesized and conducted *in vitro* characterization of photoactivatable chemiluminescence agents **UVC-454**, **UVA-**

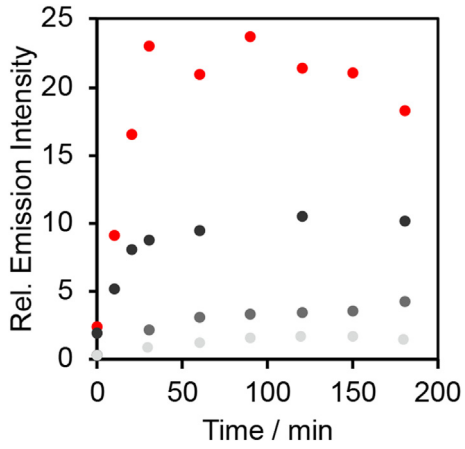

Fig. 2. UVC-454 photoactivation in water Plot of relative emission intensities measured 545 nm of 1 mM (red), 750 μM (black), 500 μM (dark gray), and 100 μM (light gray) **UVC-454** in 20 mM PBS pH 7.4 buffer and 10% Emerald II® irradiated at 254 nm in aqueous solution over 180 min. Measurements were taken in 30 min intervals. (For interpretation of the references to colour in this figure legend, the reader is referred to the web version of this article.)

454, and **Spiro-CL**. **UVC-454** and **UVA-454** undergo irreversible uncaging processes to emit light, and **Spiro-CL** acts under a reversible photoswitching mechanism governed by UV light irradiation to generate its chemiluminescent merocyanine form. Photoactivated chemiluminescence provides an attractive target for targeted imaging agents. We envision that 1,2-dioxetane probes outfitted with targeting capability such as homing peptides [75] or antibodies promote the use of *in vivo* tail vein injections that localize and build up in areas of interest. Uncaging of the chemiluminophore system using directed light excitation provides extremely high spatiotemporal control over imaging agent activity. With the production of new chemiluminescence scaffolds that emit in green [76] and red [77] regions, along with a myriad of PPGs that have uncaging abilities across the spectrum, a wide variety of photocaged chemiluminescence agents could be devised with catered uncaging and emission wavelengths. This technology could applied for formal energy upconversion applications[78] by use of PPGs that are uncaged in the NIR to far red regions to formally generate anti-Stokes emission from the photocaged chemiluminescent systems.

To our knowledge, **Spiro-CL** represents the first example of photoswitch – enabled chemiluminescence. While most 1,2-dioxetanes exhibit turn-on luminescence by caging the 1,2-dioxetane species with an activity-based reactive handle, this unique strategy enables the chemiluminophore to be self-caged, and uncaging the chemiluminescent photoswitch species allows for emission at longer wavelength than the initial input. While **Spiro-CL** represents a novel chemiluminescent scaffold modality with a unique photoswitching mechanism to initiate luminescence, due to the low chemiluminescence emission seen from **Spiro-CL**, we believe that further improvement on the photoswitching and chemiluminescence emission properties of this compound need to be explored, potentially including aforementioned encapsulation or incorporation into polymers.

4. Funding sources

The authors declare the following competing financial interest(s): A.R.L. discloses a financial stake in BioLum Sciences, LLC, a company developing chemiluminescence assays.

Author contributions

The manuscript was written through contributions of all authors. All authors have given approval to the final version of the manuscript.

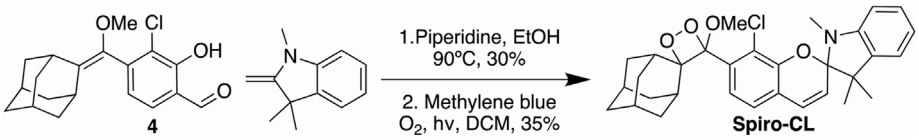

Scheme 3. Synthesis of **Spiro-CL.**

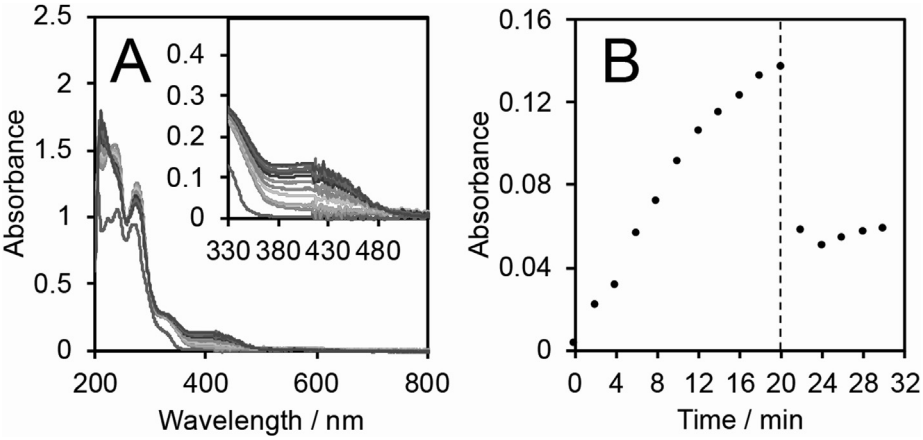

Fig. 3. UV monitoring of Spiro-CL photoswitching. (A) Absorbance of 100 μM **Spiro-CL** in EtOH upon irradiation with 254 nm light from t = 0–20 min. (B) Absorbance at 418 nm of 100 μM **Spiro-CL** in EtOH in response to 254 nm irradiation from t = 0–20 min and white light irradiation from t = 22–30 min.

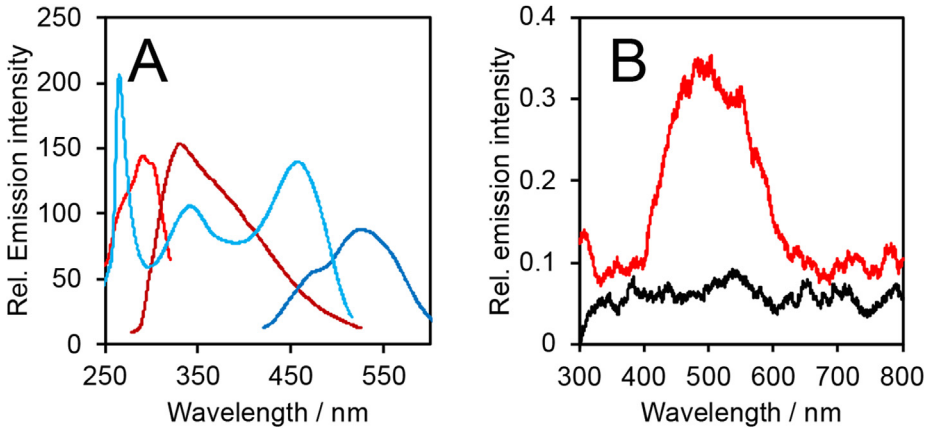

Fig. 4. Fluorescence and chemiluminescence monitoring of Spiro-CL photoswitching. (A) Fluorescence excitation and emission spectra before (red traces) and after (blue traces) 254 nm irradiation. (B) Chemiluminescence emission spectra of 10 μM **Spiro-CL** in DMSO at t = 0 (black) and 16 min (red). (For interpretation of the references to colour in this figure legend, the reader is referred to the web version of this article.)

CRediT authorship contribution statement

Lucas S. Ryan: Conceptualization, Methodology, Investigation, Writing - original draft, Writing - review & editing. **Andrew Nakatsuka:** Investigation, Writing - review & editing. **Alexander R. Lippert:** Conceptualization, Methodology, Writing - review & editing, Project administration, Funding acquisition, Supervision.

Declaration of Competing Interest

The authors declare that they have no known competing financial interests or personal relationships that could have appeared to influence the work reported in this paper.

Acknowledgment

This work was supported by the National Science Foundation under CHE 1653474.

Appendix A. Supplementary data

Supplementary data to this article can be found online at https://doi.org/10.1016/j.rechem.2021.100106.

References

[1] M. Hertzog, M. Wang, J. Mony, K. Börjesson, Strong light-matter interactions: a new direction within chemistry, Chem. Soc. Rev. 48 (2019) 937–961.
[2] J.D. Harris, M.J. Moran, I. Aprahamian, New molecular switch architectures, PNAS 115 (38) (2018) 9414–9422, https://doi.org/10.1073/pnas.1714499115.
[3] W. Szymański, J.M. Beierle, H.A.V. Kistemaker, W.A. Velema, B.L. Feringa, Reversible photocontrol of biological systems by the incorporation of molecular photoswitches, Chem. Rev. 113 (2013) 6114–6178.
[4] R.S.H. Liu, A.E. Asato, The primary process of vision and the structure of bathorhodopsin: a mechanism for photoisomerization of polyenes, Proc. Natl. Acad. Sci. 82 (1985) 259–263.
[5] N. Hasegawa, H. Jonotsuka, K. Miki, K. Takeda, X-ray structure analysis of bacteriorhodopsin at 1.3 Å resolution, Sci. Rep. 8 (2018) 1–8.
[6] F.D. Lewis, Y. Wu, X. Liu, Synthesis, structure, and photochemistry of exceptionally stable synthetic DNA hairpins with stilbene diether linkers, J. Am. Chem. Soc. 124 (2002) 12165–12173.
[7] F.D. Lewis, X. Liu, Phototriggered DNA hairpin formation in a stilbenediether-linked bis(oligonucleotide) conjugate, J. Am. Chem. Soc. 121 (1999) 11928–11929.
[8] L. Wu, K. Koumoto, N. Sugimoto, Reversible stability switching of a hairpin DNA via a photo-responsive linker unit, Chem. Commun. 1915–1917 (2009).
[9] L. Kortekaas, W.R. Browne, The evolution of spiropyran: fundamentals and progress of an extraordinarily versatile photochrome, Chem. Soc. Rev. 48 (2019) 3406–3424.
[10] P. Howlader, B. Mondal, P.C. Purba, E. Zangrando, P.S. Mukherjee, Self-assembled Pd(II) barrels as containers for transient merocyanine form and reverse thermochromism of spiropyran, J. Am. Chem. Soc. 140 (2018) 7952–7960.
[11] J. Chen, D. Wang, A. Turshatov, R. Mu, K. Landfester, One-pot fabrication of amphiphilic photoswitchable thiophene-based fluorescent polymer dots, Polym. Chem. 4 (2012) 773–781.
[12] M.E. McFadden, M.J. Robb, Force-dependent multicolor mechanochromism from a single mechanophore, J. Am. Chem. Soc. 141 (2019) 11388–11392.
[13] C. Li, Y. Zhang, J. Hu, J. Cheng, S. Liu, Reversible three-state switching of multicolor fluorescence emission by multiple stimuli modulated FRET Processes within thermoresponsive polymeric micelles, Angew. Chem. Int. Ed. 49 (2010) 5120–5124.
[14] L. Zhu, M.Q. Zhu, J.K. Hurst, A.D.Q. Li, Light-controlled molecular switches modulate nanocrystal fluorescence, J. Am. Chem. Soc. 127 (2005) 8968–8970.
[15] O. Ivashenko, J.T. Van Herpt, B.L. Feringa, P. Rudolf, W.R. Browne, UV/Vis and NIR light-responsive spiropyran self-assembled monolayers, Langmuir 29 (2013) 4290–4297.
[16] R. Klajn, Spiropyran-based dynamic materials, Chem. Soc. Rev. 43 (1) (2014) 148–184, https://doi.org/10.1039/C3CS60181A.
[17] F.M. Raymo, S. Giordani, Signal processing at the molecular level, J. Am. Chem. Soc. 123 (2001) 4651–4652.
[18] R. Rosario, D. Gust, M. Hayes, F. Jahnke, J. Springer, A.A. Garcia, Photon-modulated wettability changes on spiropyran-coated surfaces, Langmuir 18 (2002) 8062–8069.
[19] K. Wagner, R. Byrne, M. Zanoni, S. Gambhir, L. Dennany, R. Breukers, M. Higgins, P. Wagner, D. Diamond, G.G. Wallace, et al, A multiswitchable poly(terthiophene) bearing a spiropyran functionality: understanding photo- and electrochemical control, J. Am. Chem. Soc. 133 (2011) 5453–5462.
[20] D.S. Tipikin, Mechanochromism of organic compounds as exemplified by spiropyran, Russ. J. Phys. Chem. A 75 (2001) 1720–1722.
[21] W. Qiu, P.A. Gurr, G. Da Silva, G.G. Qiao, Insights into the mechanochromism of spiropyran elastomers, Polym. Chem. 10 (2019) 1650–1659.
[22] L. Kammari, T. Šolomek, B.P. Ngoy, D. Heger, P. Klán, Orthogonal photocleavage of a monochromophoric linker, J. Am. Chem. Soc. 132 (33) (2010) 11431–11433, https://doi.org/10.1021/ja1047736.
[23] J.C. Sheehan, K. Umezawa, Phenacyl photosensitive blocking groups, J. Org. Chem. 38 (1973) 3771–3774.
[24] A. Tazhe Veetil, T. Šolomek, B.P. Ngoy, N. Pavlíková, D. Heger, P. Klán, Photochemistry of S -Phenacyl Xanthates, J. Org. Chem. 76 (2011) 8232–8242.
[25] J.H. Kaplan, B. Forbush, J.F. Hoffman, Rapid Photolytic Release of Adenosine 5'-Triphosphate from a Protected Analog - Utilization by Na-K Pump of Human Red Blood-Cell Ghosts, Biochemistry 17 (1978) 1929–1935.
[26] Dunkin, I. R.; Gębicki, J.; Kiszka, M.; Sanín-Leira, D. Phototautomerism of O-Nitrobenzyl Compounds: O-Quinonoid Aci-Nitro Species Studied by Matrix Isolation and DFT Calculations. J. Chem. Soc. Perkin Trans. 2 2001, 1414–1425
[27] C.P. Holmes, Model studies for new o -nitrobenzyl photolabile linkers: substituent effects on the rates of photochemical cleavage, J. Org. Chem. 62 (1997) 2370–2380.
[28] S. Kantevari, C.J. Hoang, J. Ogrodnik, M. Egger, E. Niggli, G.C.R. Ellis-Davies, Synthesis and two-photon photolysis of 6-(Ortho-Nitroveratryl)-Caged IP3 in living cells, ChemBioChem 7 (2006) 174–180.
[29] A. Shigenaga, J. Yamamoto, Y. Sumikawa, T. Furuta, A. Otaka, Development and photo-responsive peptide bond cleavage reaction of two-photon near-infrared excitation-responsive peptide, Tetrahedron Lett. 51 (2010) 2868–2871.
[30] T. Narumi, H. Takano, N. Ohashi, A. Suzuki, T. Furuta, H. Tamamura, Isostere-based design of 8-azacoumarin-type photolabile protecting groups: a hydrophilicity-increasing strategy for coumarin-4-ylmethyls, Org. Lett. 16 (2014) 1184–1187.
[31] T. Eckardt, V. Hagen, B. Schade, R. Schmidt, C. Schweitzer, J. Bendig, Deactivation Behavior and Excited-State Properties of (Coumarin-4-Yl)Methyl Derivatives. 2.

Photocleavage of Selected (Coumarin-4-Yl)Methyl-Caged Adenosine Cyclic 3′,5′-Monophosphates with Fluorescence Enhancement, J. Org. Chem. 67 (2002) 703–710.
[32] P.P. Goswami, A. Syed, C.L. Beck, T.R. Albright, K.M. Mahoney, R. Unash, E.A. Smith, A.H. Winter, BODIPY-derived photoremovable protecting groups unmasked with green light, J. Am. Chem. Soc. 137 (2015) 3783–3786.
[33] T. Slanina, P. Shrestha, E. Palao, D. Kand, J.A. Peterson, A.S. Dutton, N. Rubinstein, R. Weinstain, A.H. Winter, P. Klán, In search of the perfect photocage: structure-reactivity relationships in meso-methyl BODIPY photoremovable protecting groups, J. Am. Chem. Soc. 139 (2017) 15168–15175.
[34] D. Kand, P. Liu, M.X. Navarro, L.J. Fischer, L. Rousso-Noori, D. Friedmann-Morvinski, A.H. Winter, E.W. Miller, R. Weinstain, Water-soluble BODIPY photocages with tunable cellular localization, J. Am. Chem. Soc. 142 (2020) 4970–4974.
[35] J.A. Peterson, C. Wijesooriya, E.J. Gehrmann, K.M. Mahoney, P.P. Goswami, T.R. Albright, A. Syed, A.S. Dutton, E.A. Smith, A.H. Winter, Family of BODIPY photocages cleaved by single photons of visible/near-infrared light, J. Am. Chem. Soc. 140 (2018) 7343–7346.
[36] D. Kand, L. Pizarro, I. Angel, A. Avni, D. Friedmann-Morvinski, R. Weinstain, Organelle-targeted BODIPY photocages: visible-light-mediated subcellular photorelease, Angew. Chem. Int. Ed. 58 (2019) 4659–4663.
[37] P. Shrestha, K.C. Dissanayake, E.J. Gehrmann, C.S. Wijesooriya, A. Mukhopadhyay, E.A. Smith, A.H. Winter, Efficient far-red/near-IR absorbing BODIPY photocages by blocking unproductive conical intersections, J. Am. Chem. Soc. 142 (2020) 15505–15512.
[38] A.P. Gorka, R.R. Nani, J. Zhu, S. Mackem, M.J. Schnermann, A near-IR uncaging strategy based on cyanine photochemistry, J. Am. Chem. Soc. 136 (2014) 14153–14159.
[39] K.C. Nicolaou, C.W. Hummel, E.N. Pitisinos, M. Nakada, A.L. Smith, K. Sibayama, H. Saimoto, Total synthesis of calicheamicin gamma, J. Am. Chem. Soc. 114 (1992) 10082–10084.
[40] Y. Gareau, R. Zamboni, A.W. Wong, Total synthesis of N-methyl LTC4: a novel methodology for the monomethylation of amines, J. Org. Chem. 58 (1993) 1582–1585.
[41] J. Walker, G.P. Reid, J.A. McCray, D.R. Trentham, Photolabile 1-(2-nitrophenyl) ethyl phosphate esters of adenine nucleotide analogues. synthesis and mechanism of photolysis, J. Am. Chem. Soc. 110 (1988) 7170–7177.
[42] A. Stutz, S. Pitsch, Automated RNA-synthesis with photocleavable sugar and nucleobase protecting groups, Synlett 1999 (Sup. 1) (1999) 930–934, https://doi.org/10.1055/s-1999-3098.
[43] J.A. Karas, D.B. Scanlon, B.E. Forbes, I. Vetter, R.J. Lewis, J. Gardiner, F. Separovic, J.D. Wade, M.A. Hossain, 2-nitroveratryl as a photocleavable thiol-protecting group for directed disulfide bond formation in the chemical synthesis of insulin, Chem. Eur. J. 20 (2014) 9549–9552.
[44] N. Ankenbruck, T. Courtney, Y. Naro, A. Deiters, Optochemical control of biological processes in cells and animals, Angew. Chem. Int. Ed. 57 (11) (2018) 2768–2798, https://doi.org/10.1002/anie.201700171.
[45] P.T. Wong, S. Tang, J. Mukherjee, K. Tang, K. Gam, D. Isham, C. Murat, R. Sun, J.R. Baker, S.K. Choi, Light-controlled active release of photocaged ciprofloxacin for lipopolysaccharide-targeted drug delivery using dendrimer conjugates, Chem. Commun. 52 (2016) 10357–10360.
[46] N.C. Fan, F.Y. Cheng, J.A.A. Ho, C.S. Yeh, Photocontrolled targeted drug delivery: photocaged biologically active folic acid as a light-responsive tumor-targeting molecule, Angew. Chem. Int. Ed. 51 (2012) 8806–8810.
[47] K.J. Bruemmer, S.W.M. Crossley, C.J. Chang, Activity-based sensing: a synthetic methods approach for selective molecular imaging and beyond, Angew. Chem. Int. Ed. 59 (2020) 13734–13762.
[48] H.J. Knox, J. Hedhli, T.W. Kim, K. Khalili, L.W. Dobrucki, J. Chan, A bioreducible N-oxide-based probe for photoacoustic imaging of hypoxia, Nat. Commun. 8 (2017) 1794.
[49] H.J. Knox, T.W. Kim, Z. Zhu, J. Chan, Photophysical tuning of N -oxide-based probes enables ratiometric photoacoustic imaging of tumor hypoxia, ACS Chem. Biol. 13 (2018) 1838–1843.
[50] E.Y. Zhou, H.J. Knox, C. Liu, W. Zhao, J. Chan, A conformationally restricted aza-BODIPY platform for stimulus-responsive probes with enhanced photoacoustic properties, J. Am. Chem. Soc. 141 (2019) 17601–17609.
[51] A.E. Albers, V.S. Okreglak, C.J. Chang, A FRET-based approach to ratiometric fluorescence detection of hydrogen peroxide, J. Am. Chem. Soc. 128 (30) (2006) 9640–9641, https://doi.org/10.1021/ja063308k.s001.
[52] C.Y.S. Chung, J.M. Posimo, S. Lee, T. Tsang, J.M. Davis, D.C. Brady, C.J. Chang, Activity-based ratiometric FRET probe reveals oncogene-driven changes in labile copper pools induced by altered glutathione metabolism, Proc. Natl. Acad. Sci. 116 (2019) 18285–18294.
[53] A.R. Lippert, G.C. Van De Bittner, C.J. Chang, Boronate oxidation as a bioorthogonal reaction approach for studying the chemistry of hydrogen peroxide in living systems, Acc. Chem. Res. 44 (2011) 793–804.
[54] M. Yang, J. Huang, J. Fan, J. Du, K. Pu, X. Peng, chemiluminescence for bioimaging and therapeutics: recent advances and challenges, Chem. Soc. Rev. 49 (2020) 6800–6815.
[55] J.M. Baumes, J.J. Gassensmith, J. Giblin, J.-J. Lee, A.G. White, W.J. Culligan, W.M. Leevy, M. Kuno, B.D. Smith, Storable, thermally activated, near-infrared chemiluminescent dyes and dye-stained microparticles for optical imaging, Nat. Chem. 2 (2010) 1025–1030.
[56] L.F.M.L. Ciscato, F.H. Bartoloni, D. Weiss, R. Beckert, W.J. Baader, Experimental evidence of the occurrence of intramolecular electron transfer in catalyzed 1,2-dioxetane decomposition, J. Org. Chem. 75 (2010) 6574–6580.
[57] W. Adam, W.J. Baader, Effects of methylation on the thermal stability and chemiluminescence properties of 1,2-dioxetanes, J. Am. Chem. Soc. 107 (1985) 410–416.
[58] F.A. Augusto, G.A. De Souza, S.P. De Souza, M. Khalid, W.J. Baader, Efficiency of electron transfer initiated chemiluminescence, Photochem. Photobiol. 89 (2013) 1299–1317.
[59] P. Farahani, M.A. Oliveira, I.F. Galván, W.J. Baader, A combined theoretical and experimental study on the mechanism of spiro-adamantyl-1,2-dioxetanone decomposition, RSC Adv. 7 (2017) 17462–17472.
[60] Vacher, M.; Fdez. Galván, I.; Ding, B.-W.; Schramm, S.; Berraud-Pache, R.; Naumov, P.; Ferré, N.; Liu, Y.-J.; Navizet, I.; Roca-Sanjuán, D.; et al. Chemi- and Bioluminescence of Cyclic Peroxides. Chem. Rev. 2018, 118, 6927-6974
[61] Joshua J. Woods, Jian Cao, Alexander R. Lippert, Justin J. Wilson, Characterization and biological activity of a hydrogen sulfide-releasing red light-activated Ruthenium(II) complex, J. Am. Chem. Soc. 140 (39) (2018) 12383–12387, https://doi.org/10.1021/jacs.8b08695.s002.
[62] J. Cao, W. An, A.G. Reeves, A.R. Lippert, A chemiluminescent probe for cellular peroxynitrite using a self-immolative oxidative decarbonylation reaction, Chem. Sci. 9 (2018) 2552–2558.
[63] L. Ryan, J. Gerberich, U. Haris, R. Mason, A. Lippert, Ratiometric PH imaging using a 1,2-dioxetane chemiluminescence resonance energy transfer sensor, ACS Sens. 5 (2020) 2925–2932.
[64] L.S. Ryan, J. Gerberich, J. Cao, W. An, B.A. Jenkins, R.P. Mason, A.R. Lippert, Kinetics-based measurement of hypoxia in living cells and animals using an acetoxymethyl ester chemiluminescent probe, ACS Sens. 4 (2019) 1391–1398.
[65] K.J. Bruemmer, O. Green, T.A. Su, D. Shabat, C.J. Chang, Chemiluminescent probes for activity-based sensing of formaldehyde released from folate degradation in living mice, Angew. Chem. Int. Ed. 57 (2018) 7508–7512.
[66] M. Yang, J. Zhang, D. Shabat, J. Fan, X. Peng, Near-infrared chemiluminescent probe for real-time monitoring singlet oxygen in cells and mice model, ACS Sens. 5 (2020) 3158–3164.
[67] M. Roth-Konforti, O. Green, M. Hupfeld, L. Fieseler, N. Heinrich, J. Ihssen, R. Vorberg, L. Wick, U. Spitz, D. Shabat, Ultrasensitive detection of salmonella and listeria monocytogenes by small-molecule chemiluminescence probes, Angew. Chem. Int. Ed. 131 (2019) 10469–10475.
[68] Y. Zhang, C. Yan, C. Wang, Z. Guo, X. Liu, W.H. Zhu, A sequential dual-lock strategy for photoactivatable chemiluminescent probes enabling bright duplex optical imaging, Angew. Chem. Int. Ed. 59 (2020) 9059–9066.
[69] S. Son, M. Won, O. Green, N. Hananya, A. Sharma, Y. Jeon, J.H. Kwak, J.L. Sessler, D. Shabat, J.S. Kim, Chemiluminescent probe for the in vitro and in vivo imaging of cancers over-expressing NQO1, Angew. Chemie Int. Ed. 58 (2019) 1739–1743.
[70] W. An, L.S. Ryan, A.G. Reeves, K.J. Bruemmer, L. Mouhaffel, J.L. Gerberich, A. Winters, R.P. Mason, A.R. Lippert, A chemiluminescent probe for HNO quantification and real-time monitoring in living cells, Angew. Chem. Int. Ed. 58 (2019) 1361–1365.
[71] W. An, R.P. Mason, A.R. Lippert, Energy transfer chemiluminescence for ratiometric PH imaging, Org. Biomol. Chem. 16 (2018) 4176–4182.
[72] J. Cao, R. Lopez, J.M. Thacker, J.Y. Moon, C. Jiang, S.N.S. Morris, J.H. Bauer, P. Tao, R.P. Mason, A.R. Lippert, Chemiluminescent probes for imaging H2S in living animals, Chem. Sci. 6 (2015) 1979–1985.
[73] T. Ueda, H. Konishi, K. Manabe, Palladium-catalyzed reductive carbonylation of aryl halides with N-formylsaccharin as a CO source, Angew. Chemie Int. Ed. 52 (2013) 8611–8615.
[74] X. Wei, X. Chen, M. Ying, W. Lu, Brain tumor-targeted drug delivery strategies, Acta Pharm. Sin. B 4 (2014) 193–201.
[75] O. Green, T. Eilon, N. Hananya, S. Gutkin, C.R. Bauer, D. Shabat, Opening a gateway for chemiluminescence cell imaging: distinctive methodology for design of bright chemiluminescent dioxetane probes, ACS Cent. Sci. 3 (2017) 349–358.
[76] O. Green, S. Gnaim, R. Blau, A. Eldar-Boock, R. Satchi-Fainaro, D. Shabat, Near-infrared dioxetane luminophores with direct chemiluminescence emission mode, J. Am. Chem. Soc. 139 (2017) 13243–13248.
[77] F. Auzel, Upconversion and anti-stokes processes with f and d ions in solids, Chem. Rev. 104 (2004) 139–173.